Thermal adaptation constrains the temperature dependence of ecosystem metabolism

Daniel Padfield[1], Chris Lowe[1,2*], Angus Buckling[1,2], Richard Ffrench-Constant[2], Elisa Schaum[1], Simon Jennings[3,4], Felicity Shelley[5], Jón S. Ólafsson[6] & Gabriel Yvon-Durocher[1*]

Author affiliations:

[1] Environment and Sustainability Institute, University of Exeter, Penryn, Cornwall, TR10 9EZ, U.K.

[2] Centre for Ecology and Conservation, College of Life and Environmental Sciences, University of Exeter, Penryn, Cornwall, TR10 9FE, U.K.

[3] Centre for Environment, Fisheries and Aquaculture Science, Lowestoft, NR33 0HT, U.K.

[4] School of Environmental Sciences, Norwich Research Park, University of East Anglia, Norwich, NR4 7TJ, U.K.

[5] School of Biological and Chemical Sciences, Queen Mary University of London, London, E1 4NS, U.K.6. Marine and Freshwater Research Institute, Árleyni 22, 112 Reykjavik, Iceland.

Corresponding authors: Gabriel Yvon-Durocher (g.yvon-durocher@exeter.ac.uk) or Chris Lowe (c.lowe@exeter.ac.uk)

Author contributions: G. Y-D. and C. L. conceived the study. D.P. and G. Y-D. designed the experimental work and D. P., G. Y-D., C. L., and BIO244 students conducted the experiments. D.P. and G. Y-D. analysed the data and all authors contributed to writing the paper. The authors declare no conflict of interest.

Data accessibility statement: All data will be made available on Dryad should the manuscript be accepted. R-Code for analysis will be available from the authors on request.

Type of Article: Letter

Number of words in: Abstract: 149; **Main Text**: 4998
Number of Figures: 3
Number of Tables: 1
Number of cited references: 50

Keywords: metabolic theory, thermal adaptation, global warming, gross primary production

ABSTRACT

Gross primary production (GPP) is the largest flux in the carbon cycle, yet its response to global warming is highly uncertain. The temperature sensitivity of GPP is directly linked to photosynthetic physiology, but the response of GPP to warming over longer timescales could also be shaped by ecological and evolutionary processes that drive variation community structure and functional trait distributions. Here, we show that selection on photosynthetic traits within and across taxa dampen the effects of temperature on GPP across a catchment of geothermally heated streams. Autotrophs from cold streams had higher photosynthetic rates and after accounting for differences in biomass among sites, rates of ecosystem-level GPP were independent of temperature, despite a 20 ºC thermal gradient. Our results suggest that thermal adaptation constrains the long-term temperature dependence of GPP, and highlights the importance of considering physiological, ecological and evolutionary mechanisms when predicting how ecosystem-level processes respond to warming.

INTRODUCTION

The carbon cycle is fundamentally metabolic (Falkowski *et al.* 2000). At the ecosystem level, gross primary production (GPP) represents the total amount of CO_2 fixed by photosynthesis into organic carbon and is the largest flux in the global carbon cycle (Beer *et al.* 2010) transferring CO_2 from the atmosphere to the biosphere, fuelling food webs and biological production (Field 1998). Understanding the mechanisms that shape how temperature influences rates of GPP across spatial, temporal and organisational scales is therefore an essential prerequisite to forecasting feedbacks between global warming and the carbon cycle.

64 Temperature can dictate rates of GPP over short timescales through its effects
65 on photosynthetic physiology (Medlyn *et al.* 2002; Allen *et al.* 2005; Galmes *et al.*
66 2015). However, it is clear that over longer timescales (e.g. decades of gradual
67 warming) ecological and evolutionary processes that mediate temperature induced
68 changes in biomass, community composition and local adaptation of metabolic traits
69 could feedback to influence the emergent effects of warming on ecosystem properties
70 (Allen *et al.* 2005; Enquist *et al.* 2007; Michaletz *et al.* 2014; Cross *et al.* 2015).
71 Indeed a recent analysis demonstrated that most of the variation in terrestrial primary
72 production along a latitudinal temperature gradient could be explained by changes in
73 biomass, and after controlling for biomass, rates were independent of temperature
74 (Michaletz *et al.* 2014). Such temperature invariance in biomass-specific rates of
75 primary production is counterintuitive considering the well-known exponential effects
76 of temperature on the biochemistry of metabolism (Gillooly *et al.* 2001). Furthermore,
77 it implies that selection on photosynthetic traits that compensate for the effects of
78 temperature on physiological rates could play a fundamental role in mediating the
79 effects of temperature on rates of primary production in the long-term (Kerkhoff *et al.*
80 2005; Enquist *et al.* 2007).

81 Here we investigate the interplay between the direct effects of temperature on
82 photosynthesis, local adaptation through selection on photosynthetic traits, and
83 changes in community biomass, on rates of gross primary production. We do so by
84 extending the general model for ecosystem metabolism from metabolic theory
85 (Enquist *et al.* 2003, 2007; Allen *et al.* 2005; Kerkhoff *et al.* 2005; Michaletz *et al.*
86 2014) to include the effects of thermal adaptation on the key traits that influence
87 individual metabolism as well as potential temperature effects on ecosystem biomass
88 pools. We then test our model's predictions against empirical data collected from a

89 catchment of naturally warmed Icelandic geothermal streams spanning a gradient of
90 20 ºC.
91
92 **THEORY**
93 The metabolic theory of ecology (MTE) provides a powerful framework for
94 understanding how temperature affects GPP by linking the photosynthetic rates of an
95 ecosystem's constituent individuals with the size and biomass structure of the
96 community (Enquist *et al.* 2003, 2007; Allen *et al.* 2005; Kerkhoff *et al.* 2005; Yvon-
97 Durocher & Allen 2012; Michaletz *et al.* 2014). Organism-level metabolism, $b(T)$,
98 responds predictably to temperature, increasing exponentially up to an optimum,
99 followed by a more pronounced exponential decline (Fig. 1a). These thermal response
100 curves can be quantified using a modification of the Sharpe-Schoolfield equation for
101 high temperature inactivation (Schoolfield *et al.* 1981):

102 $$b(T) = \frac{b(T_c) m^{\alpha} e^{E(\frac{1}{kT_c} - \frac{1}{kT})}}{1 + e^{E_h(\frac{1}{kT_h} - \frac{1}{kT})}} \quad (1)$$

103 where $b(T)$ is the rate of metabolism at temperature T, in Kelvin (K), k is
104 Boltzmann's constant (8.62×10^{-5} eV K^{-1}), E is the activation energy (in eV), E_h
105 characterises temperature-induced inactivation of enzyme kinetics above T_h, which is
106 the temperature at which half the enzymes are inactivated. In this expression, $b(T_c)$ is
107 the rate of metabolism normalised to a reference temperature (e.g. 10 ºC), where no
108 low or high temperature inactivation occurs and m^{α} is the mass dependence of
109 metabolic rate characterised by an exponent α, that ranges between ¾ and 1 across
110 multicellular and unicellular autotrophs (Gillooly *et al.* 2001; DeLong *et al.* 2010).
111 Equation 1 yields a maximum metabolic rate at an optimum temperature,

112 $$T_{opt} = \frac{E_h T_h}{E_h + k T_h ln\left(\frac{E_h}{E_p} - 1\right)} \quad (2)$$

The parameters in equations 1 & 2, which govern the height and shape of the thermal response curve can be considered "metabolic traits" (Padfield *et al.* 2016) and have long been known to shift as organisms adapt to new thermal environments (Berry & Bjorkman 1980; Huey & Kingsolver 1989). Equation 1 can be simplified to the Arrhenius equation,

$$b(T) = b(T_c)m^{\alpha}e^{E(\frac{1}{kT_c}-\frac{1}{kT})} \quad (3)$$

which captures only the rising part of the thermal response curve, if the temperatures organisms experience in the environment are below T_{opt} (Savage *et al.* 2004; Dell *et al.* 2011; Sunday *et al.* 2012). We use this simpler, more tractable model of the temperature dependence in the following theory, which attempts to explore the mechanisms driving the emergent temperature sensitivity of ecosystem-level gross primary production.

At the organism-level, the size and temperature dependence of gross photosynthesis can be characterized as:

$$gp(T) = gp(T_c)m^{\alpha}e^{E_{gp}\left(\frac{1}{kT_c}-\frac{1}{kT}\right)} \quad (4)$$

where $gp(T)$ is the rate of gross photosynthesis and temperature T, and $gp(T_c)$ is the rate of gross photosynthesis normalised to a reference temperature and E_{gp} is the activation energy of gross photosynthesis. Net photosynthesis, np, which is the amount of photosynthate available for allocation to biomass production after accounting for autotroph respiration is given by,

$$np(T) = gp(T_c)m^{\alpha}e^{E_{gp}\left(\frac{1}{kT_c}-\frac{1}{kT}\right)} - r(T_c)m^{\alpha}e^{E_r\left(\frac{1}{kT_c}-\frac{1}{kT}\right)} = np(T_c)m^{\alpha}e^{E_{np}\left(\frac{1}{kT_c}-\frac{1}{kT}\right)} \quad (5)$$

where $np(T)$ is the rate of net photosynthesis at temperature T, $r(T_c)$ is the rate of respiration normalised to a reference temperature, T_c, and E_{np} and E_r are the activation energies of net photosynthesis and respiration. The form of equation 5

implies that the temperature sensitivity of np will not strictly follow a simple Boltzmann-Arrhenius relation (see supplementary information for a derivation of E_{np}). Nevertheless, we can approximate the temperature sensitivity of net photosynthesis using an apparent activation energy, E_{np}, with a reasonable degree of accuracy (Fig. S7).

Using Equation 4 and principles from MTE, the rate of gross primary productivity per unit area, A, can be approximated by the sum of the photosynthetic rates of its constituent organisms (Fig. 1c):

$$GP_s(T) = GP(T_c)e^{E_{GP}(\frac{1}{kT_c}-\frac{1}{kT})} \quad (6)$$

where $GP_s(T)$ is the rate of gross primary production in ecosystem s, at temperature T, $GP(T_c) = \frac{1}{A}\sum_{i=1}^{J} gp_i(T_c)\, m_i^{\alpha}$, is the ecosystem-level metabolic normalisation, where J is the total number of individual organisms, i, which comprise all autotrophs in s. In equation 6, the apparent long-term temperature dependence of gross primary production, E_{GP}, is assumed to be equal to that of the average temperature dependence for individual-level gross photosynthesis, E_{gp} , provided that the ecosystem-level normalisation, $GP(T_c)$, is independent of temperature (Fig. 1d). However, if $gp_i(T_c)$ or total biomass, $M_s = \frac{1}{A}\sum_{i=1}^{J} m_i$, exhibit temperature dependence, for example via temperature driven selection on $gp_i(T_c)$ or covariance between resource availability, temperature and M_s, then the scaling of the activation energy from individuals to ecosystems will no longer hold (e.g. $E_{GP} \neq E_{gp}$). Thus, ecological processes that influence M_s and evolutionary dynamics which shape variation in $gp_i(T_c)$ have the potential to play an integral, but as yet underappreciated role in mediating the response of ecosystem metabolism to temperature if they modify the metabolic

capacity of ecosystem biomass pools (but see Kerkhoff *et al.* 2005; Enquist *et al.* 2007; Michaletz *et al.* 2014).

Previous work on aquatic and terrestrial autotrophs has shown that autotrophs adapt to long-term temperature changes by shifts in the respiratory and photosynthetic normalisation constant; up-regulating rates at low temperatures and down-regulating at high temperature, to alleviate the constraints of thermodynamics on enzyme kinetics (Atkin *et al.* 2015; Padfield *et al.* 2016; Reich *et al.* 2016; Scafaro *et al.* 2016). We therefore expect $gp_i(T_c)$ to exhibit temperature dependence along long-term thermal gradients, which in the absence of an explicit first principles derivation, we can approximate as

$$gp_i(T_c) \approx e^{E_a(\frac{1}{kT_c}-\frac{1}{kT})} \quad (7)$$

where E_a is an adaptation parameter that characterises the change in $gp_i(T_c)$ with temperature owing to thermal adaptation. Substituting the temperature dependence for $gp_i(T_c)$ into equation 6 and simplifying, yields the following expression for the temperature dependence of gross primary production,

$$GP_s(T) = GP(T_c)e^{E_a+E_{gp}(\frac{1}{kT_c}-\frac{1}{kT})} \quad (8)$$

Under the "hotter-is-better" model of thermal adaptation (Fig. 1a), where a single activation energy governs the temperature dependence of metabolism within and across species (Gillooly *et al.* 2001; Savage *et al.* 2004; Angilletta *et al.* 2010) and $E_a = 0$, the ecosystem-level activation energy would equal that of individual-level metabolism (i.e. $E_{GP} = E_{gp}$; Fig. 1d) – this is the typical assumption made in metabolic theory (Brown *et al.* 2004; Demars *et al.* 2016). However, when $E_a \neq 0$, $E_{GP} = E_a + E_{gp}$, and the ecosystem-level activation energy will deviate from the average organism-level temperature dependence owing to the effects of thermal adaptation on $gp_i(T_c)$. If thermal adaptation results in complete compensation (i.e.

$E_a = -E_{gp}$; Fig. 1b), and M_s does not covary with temperature, then ecosystem-level gross primary production will be independent of temperature (i.e. $E_{GP} = 0$; Fig. 1d). Following the same reasoning, any temperature dependence in M_s will also result in deviations from the average individual-level activation energy. For example, recent experimental work has shown that covariance between temperature and rates of nutrient cycling can cause M_s to increase with temperature (Welter *et al.* 2015; Williamson *et al.* 2016), $M_s \approx e^{E_b(\frac{1}{kT_c}-\frac{1}{kT})}$, where E_b is the activation energy characterising the temperature dependence of total biomass. When $E_b > 0$, substituting in the temperature dependence for M_s into equation 8 leads to an increase in the ecosystem-level activation energy regardless of the mode of thermal adaptation ($E_{GP} = E_{gp} + E_b + E_a$; Fig. 1d). This model emphasises how different ecological and evolutionary mechanisms that drive temperature dependent variation in individual-level metabolic traits and/or ecosystem biomass pools can influence the emergent long-term temperature sensitivity ecosystem metabolism (Fig. 1c:d).

We now use measurements of the temperature dependence of organism- and ecosystem-level photosynthesis from a catchment of naturally warmed geothermal streams to test the expectations of our model and investigate how ecological and evolutionary processes shape the long-term temperature sensitivity of GPP. Critically, this system allows us to measure photosynthetic responses to temperature at both organism and ecosystem scales from sites that are in close proximity, yet differ substantially in their thermal history (i.e. 20 ºC *in situ* temperature gradient among sites).

METHODS

Study site

The study was conducted in a geothermally active valley close to Hveragerdi village, 45 km east of Reykjavik, Iceland. The area contains a large number of mainly groundwater-fed streams that are subjected to differential natural geothermal warming from the bedrock (O'Gorman *et al.* 2014). Twelve streams have been mapped in the valley with average temperatures ranging from 7 – 27 ºC (Fig. S1 & Table S1). We measured a number of physical (width, depth, velocity) and chemical (pH, conductivity, nitrate, nitrite, soluble reactive phosphate, ammonium) variables across the stream catchment (Table S2) and none of these variables were significantly correlated with temperature (Table S3). The study was carried out during May and June in 2015 and 2016.

Measuring the population level metabolic thermal response

We sampled 13 of the most abundant autotrophic biofilm taxa from 8 streams spanning the catchment's full thermal gradient. Multiple taxa were removed from four streams where more than one taxon was at high density (Table S4). Measurements first entailed characterising a photosynthesis-irradiance (PI) curve from 0 – 2000 µmol m^{-2} s^{-1} at the average stream temperature for each taxon. Net photosynthesis (np) was measured as O_2 evolution in a Clark-type oxygen electrode (Hansatech Ltd, King's Lynn UK Chlorolab2) at increasing light intensities in intervals of 50 µmol^{-1} m^{-2} s^{-1} up to 300 µmol^{-1} m^{-2} s^{-1}, and then in intervals of 100 µmol^{-1} m^{-2} s^{-1} up to 1000 µmol^{-1} m^{-2} s^{-1}, followed by 200 µmol steps up to 2000 µmol^{-1} m^{-2} s^{-1}. Rates of respiration (r) were measured as O_2 consumption in the dark. This yielded a PI curve from which the optimal light intensity for net photosynthesis was estimated using a modification of Eilers' photoinhibition model (Eilers & Peeters 1988) fitted via non-linear least squares regression (Fig. S2):

$$np(I) = \frac{np_{max} I}{(np_{max}/\alpha {I_{opt}}^2)\, I^2 + \left(1 - \left(\frac{2np_{max}}{\alpha I_{opt}}\right)\right) I + \frac{np_{max}}{\alpha}} - r \quad (9)$$

where $np(I)$, is the rate of net photosynthesis at irradiance, I, np_{max} is the photosynthetic maximum that occurs at optimal light, I_{opt}, α controls the gradient of the initial slope and r is respiration, the rate of oxygen consumption in the dark. The optimum light intensity (I_{opt}, µmol^{-1} m^{-2} s^{-1}) for each taxon was then used for measuring net photosynthesis at all other assay temperatures in the acute thermal gradient experiments. Rates of gross photosynthesis were calculated by the summation of the measured rates of net photosynthesis and respiration.

Rates of photosynthesis and respiration were normalised to biomass by expressing rates per unit of chlorophyll *a*. Chlorophyll *a* extraction was achieved by grinding the sample tissue with methanol for 5 minutes, centrifugation and measuring chlorophyll *a* extinction coefficients on a spectrophotometer. Total chlorophyll *a* (µg) was then calculated by measuring absorbance at 750 nm, 665 nm and 632 nm.

$$\text{Chl } a = (13.26(A_{665} - A_{750}) - 2.68(A_{665} - A_{750})) \times 10^{-3} \quad (10)$$

Acute temperature responses of biomass normalised gross and net photosynthesis and respiration were fitted to the modified Sharpe-Schoolfield equation for high temperature inactivation (Equation 1). Best fits for each thermal response curve were determined using non-linear least squares regression using the 'nlsLM' function in the 'minpack.lm' (Elzhov *et al.* 2009) package in R statistical software (R Core Team 2014; v3.2.2), following the methods outlined in Padfield *et al.*, (2016).

We tested for thermal adaptation by assessing whether the parameters in eqns. 1 and 2 as well as the rate of gross photosynthesis at the average stream temperature, $gp(T_s)$ varied systematically with stream temperature. We fitted the metabolic traits

to a modified Boltzmann-Arrhenius function within a linear mixed effects modelling framework:

$$\ln z(T) = \ln z(T_c) + E_a \left(\frac{1}{kT_c} - \frac{1}{kT}\right) + \varepsilon^t \quad (11)$$

where z is the metabolic trait at stream temperature, T, $z(T_c)$ is the value of the trait at the mean temperature across all streams, T_c, and E_a is the activation energy that determines how much z changes as a function of T due to thermal adaptation and ε^t is a random effect on the intercept accounting for multiple measurements of the same metabolic trait of each isolated biofilm taxon (i.e. one value each for gross and net photosynthesis and respiration). We fitted eq. 11 to each metabolic trait with stream temperature, flux (3 level factor with 'gross' and 'net photosynthesis' and 'respiration') and their interaction as fixed effects (Table S5). Significance of the parameters were determined using likelihood ratio tests. Model selection was carried out on models fitted using maximum likelihood and the most parsimonious model was refitted using restricted maximum likelihood for parameter estimation.

Measuring *in situ* rates of ecosystem-level gross primary production

Ecosystem metabolism was calculated from measurements of dissolved oxygen over time using the single station method (Odum 1956). Sensors were deployed in all streams and at multiple sites within a stream where temperature gradients existed within streams due to differential geothermal warming. Dissolved oxygen concentration and temperature were monitored at 1-minute intervals using miniDOT dissolved oxygen loggers (PME Inc) (Fig. S3 & Fig. S5). Light sensors **(**LI-COR Inc**)** were deployed simultaneously at two sites in the centre of the catchment. Physical variables of each stream, including the depth (m), width (m), velocity (m s^{-1}), were measured along horizontal transects at 10 m intervals up to 100 m upstream of the

284 sensor deployment. Values for depth, width and velocity were averaged across the
285 reach (Table S2).

286 The change in O_2 concentration at a single station between two subsequent
287 measurements (ΔDO) can be approximated as:

288 $$\Delta\, DO = \frac{[O_2]_t - [O_2]_{t-1}}{\Delta t} \quad (12)$$

289 with $[O_2]_t$ the concentration of oxygen (mg L^{-1}) at time t and can be modelled using a
290 framework based on the Odum's O_2 change technique (Odum 1956):

291 $$\Delta\, DO = GPP - ER \pm K \quad (13)$$

292 where GPP (g m^{-3} hr^{-1}) is the composite of volumetric gross primary productivity,
293 minus volumetric ecosystem respiration, ER (g m^{-3} hr^{-1}) and K is the net exchange of
294 oxygen with the atmosphere (g O_2 m^{-3}). The net exchange of oxygen with the
295 atmosphere is the product of the O_2 gas transfer velocity, k (m min^{-1}), and the O_2
296 concentration gradient between the water body and the atmosphere (temperature and
297 atmosphere corrected DO concentration at 100% saturation minus $[O_2]_t$) over the
298 measurement interval.

299 The gas transfer velocity, k (m min^{-1}), was calculated using the surface-
300 renewal model and corrected for the stream temperature:

301 $$k = 50.8\, V^{0.67} \times D^{-0.85} \times 1.024^{(T-20)} \quad (14)$$

302 where V is velocity (cm s^{-1}), D is the mean stream depth (cm) adjusted for stream
303 temperature, T (Bott 1996). This value was subsequently transformed into (m h^{-1}).
304 Estimated rates of reaeration, derived using the surface renewal model from
305 measurements of velocity and depth, correspond well to reaeration rates measured
306 experimentally using propane additions in an adjacent Icelandic catchment with
307 comparable physico-chemical characteristics (see Fig. S8; Demars *et al.* 2011).

The net metabolic flux for a given measurement interval is equal to $\Delta DO - K$. During the night (where light < 5 µmol m^{-2} s^{-1}), GPP is zero, so the net metabolic flux is equal to ER. During the day, ER was determined by interpolating average ER over the defined night period. GPP for each daytime interval was the difference between net metabolism flux and interpolated ER. Daily volumetric rates of GPP (g O_2 m^{-3} day^{-1}) were calculated as the sum of the 15-minute rates over each 24-hour period. Volumetric rates were converted to areal units (g O_2 m^{-2} day^{-1}) by multiplying by the mean water depth of the stream reach.

We measured autotrophic biomass density (g Chl *a* m^{-2}) across the stream catchment by taking measurements of chlorophyll *a*. A core of 28.27 cm^2 was removed from 3 randomly chosen rocks and chlorophyll *a* was measured using the extraction protocol detailed above. The total standing biomass, M_s, of each stream reach was estimated by multiplying average biomass density by the total reach area, which was estimated from the mean width and the distance upstream from the oxygen sensor integrated over (Chapra & Di Toro 1991; Demars *et al.* 2015),

$$d = \frac{3v}{k_2} \quad (15)$$

where three times the velocity of the stream (v; m d^{-1}) divided by the gas transfer coefficient (K_2; d^{-1}) gives the approximation of the distance upstream integrated by the single station method (d; m) (Grace & Imberger 2006). Biomass normalised rates of GPP per stream (g O_2 g Chl a^{-1} day^{-1}) were calculated by dividing areal rates of GPP by the total standing biomass in the upstream reach.

We used linear mixed-effects modelling to investigate the temperature dependence of GPP across catchment, allowing us to control for the hierarchical structure of the data (e.g. variance of days nested within years nested within streams).

We characterised the temperature dependence of GPP with a linearised version of the Boltzmann-Arrhenius function in a linear mixed effects model:

$$\ln GP_s(T) = E_{GP}\left(\frac{1}{kT_c} - \frac{1}{kT}\right) + (\langle \ln GP(T_c)\rangle + \varepsilon_P^{s/y/d}) \quad (16)$$

where $GP_s(T)$ is the rate of gross primary production in stream *s* on year *y* on day *d* at temperature T (Kelvin), E_{GP} is the activation energy (eV) which characterises the exponential temperature sensitivity of photosynthetic rates, $\langle \ln GP(T_c) \rangle$ is the average rate of GP across streams and days normalised to T_c = 283 K (10 ºC) and $\varepsilon_P^{s/y/d}$ is a nested random effect that characterises deviations from $\langle \ln GP(T_c) \rangle$ at the level of *d* within *y* within *s*. Significance of the parameters and model selection was carried out as described above for the analysis of the population-level metabolic traits (Table 1).

We tested for the effect of total biomass and temperature on GPP across the catchment using the data from 2016 (where we also quantified autotroph biomass) by undertaking a multiple regression by expanding eq. 16 to include the effect the biomass on GPP:

$$\ln GP(T) = E_{GP}\left(\frac{1}{kT_c} - \frac{1}{kT}\right) + \beta \ln M_s + (\langle \ln GP(T_c)\rangle + \varepsilon_P^{s/d}) \quad (17)$$

where β characterises the power-law scaling of $GP(T)$ with M_s and the random effects specification changed to account for deviation from $\langle \ln GP(T_c)\rangle$ between days nested within streams. Model selection was as described above (Table 1).

Inorganic nutrients

Water samples for measuring dissolved inorganic nutrient concentrations (NO_2, NO_3, NH_4 and PO_4; μmol L^{-1}) were collected from each stream. Samples were filtered (Whatmann GF/F) and stored frozen at -20 ºC for subsequent analysis using a segmented flow auto-analyser (Table S3) (Kirkwood 1996).

356

357 **RESULTS**

358 **Population level metabolism**

359 Macroscopic cyanobacteria, filamentous eukaryotic algae, and bryophytes were the
360 dominant autotrophs across the catchment (Table S4). To investigate how long-term
361 differences in temperature shaped variation in photosynthetic traits across the
362 catchment, we sampled the most abundant autotroph taxa from 8 streams spanning the
363 full temperature gradient and measured the acute responses of gross photosynthesis
364 and respiration to temperatures spanning 5 to 50 ºC. Gross photosynthesis and
365 respiration followed unimodal responses to acute temperature variation and were well
366 fit by equation 1 (Fig. 2a-b). We predicted exponential declines in the metabolic
367 normalisation constants, moving from cold to warm environments, owing to the
368 effects of thermal adaptation. Consistent with this hypothesis, the log-transformed
369 rates of gross photosynthesis, ($\ln gp(T_c)$) and respiration ($\ln r(T_c)$) normalised to a
370 reference temperature, T_c = 10 ºC, declined linearly with increasing stream
371 temperature with the same activation energy (E_a = -0.64 eV; 95% CI: -1.22 to -0.05
372 eV; Fig. 2c). Since $np(T_c) = gp(T_c) - r(T_c)$, the normalisation for net
373 photosynthesis also declined with increasing temperature with an E_a = -0.64 eV.

374 Because the dominant autotroph taxa varied across the streams (Table S4), the
375 decline in the photosynthetic trait, $gp(T_c)$, with increasing stream temperature is
376 likely influenced by species sorting (e.g. filtering of species and traits from the
377 regional species pool). To investigate whether adaptive evolution also played a role,
378 we analysed data from only the most common genera *Nostoc,* which was distributed
379 across 5 streams spanning a gradient of 10.2 ºC. $gp(T_c)$, $np(T_c)$ and $r(T_c)$ also
380 decreased with increasing stream temperature in *Nostoc* with the thermal sensitivity

not significantly different from that of all the autotroph taxa together (Fig. S6). This trend provides evidence for local thermal adaptation. An important consequence of the decrease in $gp(T_c)$ with increasing stream temperature was that rates of gross photosynthesis at the average temperature of each stream, $gp(T_s)$, were independent of temperature (Fig. 2d), indicating that species sorting and adaptation led to complete compensation of organism-level metabolism over the catchment's thermal gradient.

Both the optimum temperature, T_{opt}, and T_h, which is the temperature at which half the enzymes are inactivated, were positively correlated with average stream temperature (Table S5) providing further evidence for local adaptation. We found no evidence for systematic variation in the activation or inactivation energies (E_a or E_h) across the thermal suggesting these traits are unlikely to be under temperature dependent-selection (Table S5). Previous work has often shown that photosynthesis has a lower activation energy than respiration (Allen *et al.* 2005; López-Urrutia *et al.* 2006; Padfield *et al.* 2016). In contrast, we found that the average activation energies of gross photosynthesis and respiration were not significantly different and could be characterised by a common activation energy, E = 0.87 eV; 95% CI = 0.77 to 0.97 eV. Similarly, E_h, which characterises inactivation of kinetics past the optimum was not significantly different between fluxes and could be characterised by a common value for respiration and photosynthesis (E_h = 4.91 eV; 95% CI: 3.95 – 5.97 eV).

Ecosystem level gross primary productivity

Based on the observation that the activation energies of gross photosynthesis and the adaptation parameter were of equal magnitude and opposite sign, our model for the scaling of metabolism from organisms to ecosystems (Eq. 8) predicts that rates of

406 gross primary production should be independent of temperature across the catchment
407 (e.g. $E_{GP} = E_{gp} + E_a \approx 0$), provided that biomass does not covary with temperature.
408 We measured rates of *in situ* GPP in 11 streams across the catchment's full
409 temperature gradient in 2015 and 2016. Rates of GPP increased with average stream
410 temperature and the long-term temperature sensitivity of GPP (characterised by fitting
411 the Boltzmann-Arrhenius function [see Methods]) yielded an activation energy of
412 E_{GP}= 0.57 eV (95% CI: 0.10 – 1.04 eV; Fig. 3a).

413 To investigate potential covariance between temperature and biomass, M_s, and
414 its impact on the temperature dependence of GPP, we also quantified *in situ* standing
415 autotrophic biomass. Autotroph biomass density, M_s, increased systematically with
416 temperature across the catchment with a temperature sensitivity of E_b = 0.68 eV (95%
417 CI: 0.24 – 1.12 eV; Fig. 3b). The similarity between E_{GP} and E_b – they have 95%
418 confidence intervals that overlap – indicates that covariance between biomass and
419 temperature could be the main driver of the temperature dependence of GPP across
420 the catchment.

421 We quantified the effects of both temperature and M_s on GPP using multiple
422 regression in a mixed effects modelling framework (see Methods). The best fitting
423 model included only ln (M_s) as a predictor (Table 1; Fig. 3c) and after controlling for
424 variation in ln (M_s), rates of GPP were independent of temperature across the
425 catchment (Table 1; Fig. 3d). These findings are consistent with predictions from our
426 model and provide evidence that systematic variation in the photosynthetic
427 normalisation owing to thermal adaptation results in complete compensation of
428 biomass-specific metabolic rates at organism and ecosystem scales.

429

430 **Discussion**

Understanding how ecosystem-level properties like gross primary production (GPP) will respond to global warming is of central importance to predicting the response of the carbon cycle and contributing biogeochemical and food web processes to climate change. It is however a major challenge that requires an integration of physiological, ecological and evolutionary processes that together shape the emergent response of ecosystem metabolism to long-term changes in temperature. We have addressed this key problem by extending the general model of ecosystem metabolism from metabolic theory (Enquist *et al.* 2003, 2007; Allen *et al.* 2005; Kerkhoff *et al.* 2005) and testing its predictions at organism and ecosystem scales in a catchment of naturally warmed geothermal streams. Our model and analyses demonstrate that temperature-dependent selection on organism-level metabolic traits and shifts in ecosystem biomass can be as important as the direct effects of temperature on metabolism in shaping the temperature dependence of GPP.

Our model predicted that when the temperature dependence of the metabolic normalisation constant across taxa inhabiting environments with different thermal histories is of a similar magnitude but opposing sign to that of organism-level metabolism, the two temperature sensitivities cancel, rendering biomass-specific metabolic rates independent of temperature. Measurements of the thermal response curves for photosynthesis and respiration from the autotrophs isolated across the 20 ºC *in situ* gradient provided strong support for this prediction, with rates of gross photosynthesis invariant with respect to differences in average *in situ* temperatures and activation energies of organism-level gross photosynthesis and the photosynthetic normalisation, $gp(T_c)$, across taxa that were not significantly different and of opposite sign.

455 The exponential decline in $gp(T_c)$ along the *in situ* thermal gradient primarily
456 reflected turnover in the composition of the dominant autotroph taxa across the
457 streams driven by species sorting. This result is in line with work demonstrating
458 declines in the metabolic normalisation constant across vascular plant species along
459 broad-scale latitudinal gradients in terrestrial ecosystems (Atkin *et al.* 2015).
460 However, we also found a comparable negative temperature dependence of $gp(T_c)$ in
461 the genera, *Nostoc*, which was distributed across 5 streams, indicating that
462 evolutionary adaptation within taxa was also an important determinant of variation in
463 this key trait among sites in our study. This finding is consistent with work
464 demonstrating down-regulation of the metabolic normalisation in a unicellular alga
465 via rapid (e.g. over 100 generations or 45 days) evolutionary adaptation to an
466 experimental thermal gradient in the laboratory (Padfield *et al.* 2016). Collectively,
467 this work highlights that changes in the metabolic normalisation result from
468 temperature-driven selection both within and across species and can give rise to
469 temperature invariance of metabolic rates along thermal gradients (Fig. 1b).

470 Our work shows that the mode of thermal adaptation, in driving complete
471 temperature compensation of organism-level metabolism, had important implications
472 for understanding the temperature dependence of ecosystem-level GPP across the
473 catchment. GPP increased with temperature across the catchment (Fig. 3a), but it did
474 so because biomass also positively covaried with temperature (Fig. 3b). After
475 accounting for biomass, GPP was independent of temperature (Fig. 3c), consistent
476 with the effects of thermal adaptation in driving temperature compensation of
477 organism-level metabolism. These findings confirm the predictions of our model and
478 previous suggestions (Kerkhoff *et al.* 2005; Enquist *et al.* 2007) that local adaptation
479 of metabolic traits can yield the paradoxical phenomenon that rates of ecosystem

480 metabolism are independent of temperature over thermal gradients that have been
481 maintained over long timescales.

482 A great deal of empirical and theoretical work is still required to develop a
483 complete, general theory that predicts how ecosystem properties emerge from
484 evolutionary and community processes. Our work adds to recent efforts to this end
485 (Enquist *et al.* 2007; Yvon-Durocher & Allen 2012; Schramski *et al.* 2015) by
486 showing how temperature dependence of ecosystem biomass and the organism-level
487 photosynthetic normalisation alter the emergent temperature sensitivity of ecosystem-
488 level GPP. One important gap in the theory presented here is a mechanistic model for
489 the temperature dependence of the metabolic normalisation owing to thermal
490 adaptation. Our representation in equation 7 is merely a statistical description of an
491 empirical phenomenon. The metabolic cold adaptation hypothesis seeks to explain the
492 observation that species from cold environments often have higher mass-specific
493 metabolic rates compared to counterparts from warmer regions as an evolutionary
494 adaptation to compensate for lower biochemical reaction rates (Addo-Bediako *et al.*
495 2002). However, a quantitative, first principles derivation of this pattern remains
496 elusive. Recent work on autotrophs has proposed that down-regulation of respiration
497 rates as organisms adapt to warmer environments is driven by a necessity to maintain
498 the carbon-use efficiency above a threshold when rates of respiration are more
499 sensitive to temperature than those of photosynthesis (Padfield *et al.* 2016). Yet, as
500 we have shown here, the assumption that the activation energy of respiration is
501 always larger than that of photosynthesis does not always hold.

502 A better understanding of the mechanisms that give rise to the emergence of
503 ecosystem properties is central to improving predictions of how global warming will
504 alter the feedbacks between the biosphere on the carbon cycle (Levin 1998; Ziehn *et*

505 *al.* 2011; Booth *et al.* 2012). Incorporating evolution into earth system and ecosystem
506 models should be considered as a priority, especially in light of our finding that
507 thermal adaptation can completely override the direct effects of temperature on
508 metabolic rates. However, despite much recent progress (Smith & Dukes 2013;
509 Daines *et al.* 2014; Smith *et al.* 2016), substantial work remains.

510 We capitalised on a 'natural experiment' using a geothermally heated stream
511 catchment to show that thermal adaptation of photosynthesis drives an equivalence in
512 biomass normalised GPP over a 20 ºC *in situ* temperature gradient. Our results
513 suggest that local thermal adaptation plays a key role in determining how metabolic
514 rates scale from populations to ecosystems and questions the assumption that the
515 effects of temperature on enzyme kinetics can be applied to assess the long-term
516 effects of temperature on ecosystem metabolism (Demars *et al.* 2016). They also shed
517 light on the way in which the interplay between ecological and evolutionary processes
518 could influence the response of the carbon cycle, and hence constituent food web and
519 biogeochemical processes, to future environmental change.

520

521 **References**

522

523 1.Addo-Bediako, A., Chown, S.L. & Gaston, K.J. (2002). Metabolic cold adaptation
524 in insects : a large-scale perspective. *Funct. Ecol.*, 332–338

525

526 2.Allen, A.P., Gillooly, J.F. & Brown, J.H. (2005). Linking the global carbon cycle to
527 individual metabolism. *Funct. Ecol.*, 19, 202–213

528

529 3.Angilletta, M.J., Huey, R.B. & Frazier, M.R. (2010). Thermodynamic effects on

organismal performance: is hotter better? *Physiol. Biochem. Zool. Ecol. Evol. Approaches*, 83, 197–206

4.Atkin, O.K., Bloomfield, K.J., Reich, P.B., Tjoelker, M.G., Asner, G.P., Bonal, D., *et al.* (2015). Global variability in leaf respiration in relation to climate , plant functional types and leaf traits. *New Phytol.*, 206, 614–636

5.Beer, C., Reichstein, M., Tomelleri, E., Ciais, P., Jung, M. & Carvalhais, N. (2010). Terrestrial gross carbon dioxide uptake: Global distribution and covariation with climate. *Science*, 329, 834–839

6.Berry, J. & Bjorkman, O. (1980). Photosynthetic response and adaptation to temperature in higher plants. *Annu. Rev. Plant Physiol.*, 31, 491–543

7.Booth, B.B.B., Jones, C.D., Collins, M., Totterdell, I.J., Cox, P.M., Sitch, S., *et al.* (2012). High sensitivity of future global warming to land carbon cycle processes. *Environ. Res. Lett.*, 7, 24002

8.Bott, T. (1996). Primary productivity and community respiration. In: *Methods stream Ecol. Elsevier Acad. Press*. San Diego

9.Brown, J., Gillooly, J., Allen, A., Savage, V. & West, G. (2004). Toward a metabolic theory of ecology. *Ecology*, 85(7), 1771–1789

10.Chapra, S. & Di Toro, D. (1991). Delta method for estimating primary production,

555 respiration, and reaeration in streams. *J. Environ. Eng.*, 117, 640–655

556

557 11.Cross, W.F., Hood, J.M., Benstead, J.P., Huryn, A.D. & Nelson, D. (2015).
558 Interactions between temperature and nutrients across levels of ecological
559 organization. *Glob. Chang. Biol.*, 21, 1025–1040

560

561 12.Daines, S., Clark, J. & Lenton, T. (2014). Multiple environmental controls on
562 phytoplankton growth strategies determine adaptive responses of the N : P ratio. *Ecol.*
563 *Lett.*, 17, 414–425

564

565 13.Dell, A.I., Pawar, S. & Savage, V.M. (2011). Systematic variation in the
566 temperature dependence of physiological and ecological traits. *Proc. Natl. Acad. Sci.*
567 *U. S. A.*, 108, 10591–6

568

569 14.DeLong, J.P., Okie, J.G., Moses, M.E., Sibly, R.M. & Brown, J.H. (2010). Shifts
570 in metabolic scaling, production, and efficiency across major evolutionary transitions
571 of life. *Proc. Natl. Acad. Sci. U. S. A.*, 107, 12941–5

572

573 15.Demars, B.O.L., Gíslason, G.M., Ólafsson, J.S., Manson, J.R., Friberg, N., Hood,
574 J.M., *et al.* (2016). Impact of warming on CO_2 emissions from streams countered by
575 aquatic photosynthesis. *Nat. Geosci.*, 9, 758–761

576

577 16.Demars, B.O.L., Russell Manson, J., Ólafsson, J.S., Gíslason, G.M.,
578 Gudmundsdóttir, R., Woodward, G., *et al.* (2011). Temperature and the metabolic
579 balance of streams. *Freshw. Biol.*, 56, 1106–1121

17.Demars, B.O.L., Thompson, J. & Manson, J.R. (2015). Stream metabolism and the open diel oxygen method: Principles, practice, and perspectives. *Limnol. Oceanogr. Methods*, 13, 356–374

18.Eilers, P.H. & Peeters, J.C. (1988). A model for the relationship between light intensity and the rate of photosynthesis in phytoplankton. *Ecol. Modell.*, 42, 199–215

19.Elzhov, T., Mullen, K. & Bolker, B. (2009). minpack. lm: R Interface to the Levenberg-Marquardt Nonlinear Least-Squares Algorithm Found in MINPACK. *R Package version*

20.Enquist, B.J., Economo, E.P., Huxman, T.E., Allen, A.P., Ignace, D.D. & Gillooly, J.F. (2003). Scaling metabolism from organisms to ecosystems. *Nature*, 423, 639–42

21.Enquist, B.J., Kerkhoff, A.J., Huxman, T.E. & Economo, E.P. (2007). Adaptive differences in plant physiology and ecosystem paradoxes: Insights from metabolic scaling theory. *Glob. Chang. Biol.*, 13, 591–609

22.Falkowski, P., Scholes, R.J., Boyle, E., Canadell, J., Canfield, D., Elser, J., *et al.* (2000). The global carbon cycle : A test of our knowledge of earth as a system. *Science*, 290, 291–297

23.Field, C.B. (1998). Primary production of the biosphere: Integrating terrestrial and oceanic components. *Science*, 281, 237–240

24.Galmes, J., Kapralov, M., Copolovici, L., Hermida-Carrera, C. & Niinemets, U. (2015). Temperature responses of the Rubisco maximum carboxylase activity across domains of life : phylogenetic signals , trade-offs , and importance for carbon gain. *Photosynth. Res.*, 123, 183–201

25.Gillooly, J.F., Brown, J.H., West, G.B., Savage, V.M. & Charnov, E.L. (2001). Effects of size and temperature on metabolic rate. *Science*, 293, 2248–51

26. Grace, M.R and Imberger, S.J. "Stream Metabolism: Performing & Interpreting Measurements". *Water Studies Centre Monash University, Murray Darling Basin Commission and New South Wales Department of Environment and Climate Change* (2006).

27.Huey, R.B. & Kingsolver, J.G. (1989). Evolution of thermal sensitivity of ectotherm performance. *Trends Ecol. Evol.*, 4, 131–135

28.Kerkhoff, A.J., Enquist, B.J., Elser, J.J. & Fagan, W.F. (2005). Plant allometry, stoichiometry and the temperature-dependence of primary productivity. *Glob. Ecol. Biogeogr.*, 14

29.Kirkwood, D. (1996). Nutrients: practical notes on their determination in seawater. *ICES Tech. Mar. Environ. Sci.*

30.Levin, S.A. (1998). Ecosystems and the biosphere as complex adaptive systems.

630 *Ecosystems*, 1, 431–436

631

632 31.López-Urrutia, A., San Martin, E., Harris, R.P. & Irigoien, X. (2006). Scaling the

633 metabolic balance of the oceans. *Proc. Natl. Acad. Sci. U. S. A.*, 103, 8739–8744

634

635 32.Medlyn, B.E., Dreyer, E., Ellsworth, D., Forstreuter, M., Harley, P.C.,

636 Kirschbaum, M.U.F., *et al.* (2002). Temperature response of parameters of a

637 biochemically based model of photosynthesis . II . A review of experimental data, 61,

638 1167–1179

639

640 33.Michaletz, S.T., Cheng, D., Kerkhoff, A.J. & Enquist, B.J. (2014). Convergence of

641 terrestrial plant production across global climate gradients. *Nature*, 512, 39–43

642

643 34.O'Gorman, E.J., Benstead, J.P., Cross, W.F., Friberg, N., Hood, J.M., Johnson,

644 P.W., *et al.* (2014). Climate change and geothermal ecosystems: Natural laboratories,

645 sentinel systems, and future refugia. *Glob. Chang. Biol.*, 20, 3291–3299

646

647 35.Odum, H.T. (1956). Primary production in flowing waters. *Limnol. Oceanogr.*, 1,

648 102–117

649

650 36.Padfield, D., Yvon-durocher, G., Buckling, A., Jennings, S. & Yvon-durocher, G.

651 (2016). Rapid evolution of metabolic traits explains thermal adaptation in

652 phytoplankton. *Ecol. Lett.*, 19, 133–142

653

654 37.Reich, P.B., Sendall, K.M., Stefanski, A., Wei, X., Rich, R.L. & Montgomery,

655 R.A. (2016). Boreal and temperate trees show strong acclimation of respiration to
656 warming. *Nature*, 531, 633–636
657
658 38.Savage, V.M., Gillooly, J.F., Brown, J.H. & Charnov, E.L. (2004). Effects of body
659 size and temperature on population growth. *Am. Nat.*, 163, 429–41
660
661 39.Scafaro, A.P., Xiang, S., Long, B.M., Bahar, N.H.A., Weerasinghe, L.K., Creek,
662 D., *et al.* (2016). Strong thermal acclimation of photosynthesis in tropical and
663 temperate wet-forest tree species: the importance of altered Rubisco content. *Glob.*
664 *Chang. Biol.*
665
666 40.Schoolfield, R.M., Sharpe, P.J. & Magnuson, C.E. (1981). Non-linear regression
667 of biological temperature-dependent rate models based on absolute reaction-rate
668 theory. *J. Theor. Biol.*, 88, 719–731
669
670 41.Schramski, J.R., Dell, A.I., Grady, J.M., Silby, R.M. & Brown, J.H. (2015).
671 Metabolic theory predicts whole-ecosystem properties. *PNAS*, 112, 2617–2622
672
673 42.Smith, N.G. & Dukes, J.S. (2013). Plant respiration and photosynthesis in global-
674 scale models: incorporating acclimation to temperature and CO_2. *Glob. Chang. Biol.*,
675 19, 45–63
676
677 43.Smith, N.G., Malyshev, S.L., Shevliakova, E., Kattge, J. & Dukes, J.S. (2016).
678 Foliar temperature acclimation reduces simulated carbon sensitivity to climate. *Nat.*
679 *Clim. Chang.*, 6, 407–411

680

681 44.Sunday, J.M., Bates, A.E. & Dulvy, N.K. (2012). Thermal tolerance and the global

682 redistribution of animals. *Nat. Clim. Chang.*, 2, 1–5

683

684 45.Team, R.C. (2014). R: A language and environment for statistical computing. R

685 Foundation for Statistical Computing, Vienna, Austria, 2012

686

687 46.Welter, J.R., Benstead, J.P., Cross, W.F., Hood, J.M., Huryn, A.D., Johnson, P.W.,

688 *et al.* (2015). Does N_2 fixation amplify temperature dependence of ecosystem

689 metabolism? *Ecology*, 96, 603–610

690

691 47.Williamson, T.J., Cross, W.F., Benstead, J.P., Gíslason, G.M., Hood, J.M., Huryn,

692 A.D., *et al.* (2016). Warming alters coupled carbon and nutrient cycles in

693 experimental streams. *Glob. Chang. Biol.*, 22, 2152–2164

694

695 48.Yvon-Durocher, G. & Allen, A.P. (2012). Linking community size structure and

696 ecosystem functioning using metabolic theory. *Philos. Trans. R. Soc. Lond. B. Biol.*

697 *Sci.*, 367, 2998–3007

698

699 49.Yvon-Durocher, G., Allen, A.P., Bastviken, D., Conrad, R., Gudasz, C., St-Pierre,

700 A., *et al.* (2014). Methane fluxes show consistent temperature dependence across

701 microbial to ecosystem scales. *Nature*, 507, 488–491

702

703 50.Ziehn, T., Kattge, J., Knorr, W. & Scholze, M. (2011). Improving the

704 predictability of global CO_2 assimilation rates under climate change. *Geophys. Res.*

Lett., 38, 1–5

Acknowledgments: We thank Benoit Demars for providing reaeration data and comments that signficantly improved the manuscript. This study was supported a NERC Case studentship awarded to DP, GYD and SJ, an ERC starting grant awarded to GYD, and the University of Exeter.

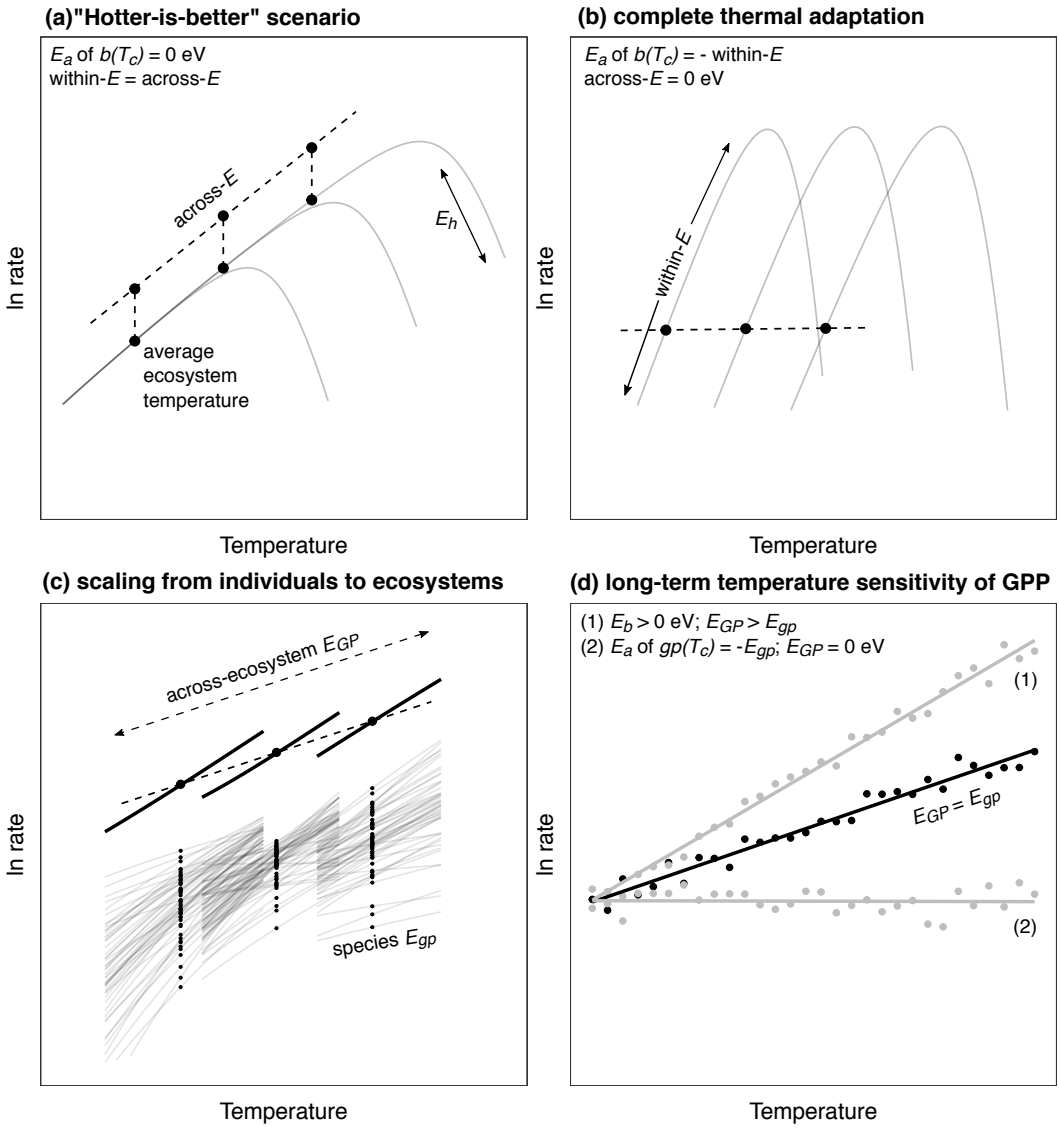

Figure 1 | Scaling metabolism from organisms to ecosystems. (a) In a "hotter-is-better" scenario, thermodynamic constraints entirely dictate individual metabolic rates such that adaptation can only occur by moving peak performance up and down an "across-species" thermal performance curve. (b) Under complete thermal adaptation, an equalisation of peak rates occurs through upregulation of metabolic rates at cold, and downregulation of rates at high temperatures. (c) The long-term ecosystem temperature response, E_{GP}, is an emergent property dependent on the thermal response of each ecosystem's constituent individuals. (d) If local thermal adaptation drives temperature dependence in the metabolic normalisation (e.g. as expected under the 'complete thermal adaptation' hypothesis) or standing biomass is temperature dependent, the long-term temperature sensitivity of ecosystem metabolism may deviate away from the average activation energy of individual metabolism.

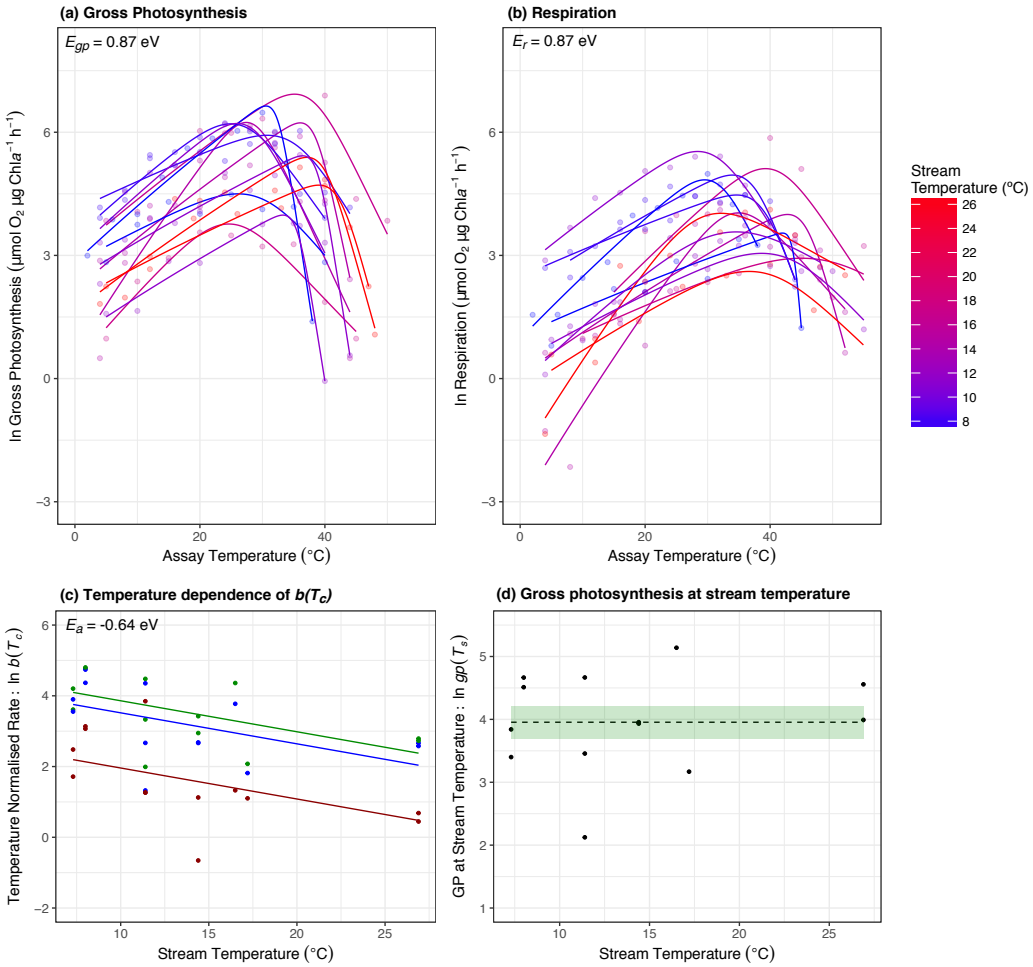

Figure 2 | Patterns of metabolic thermal adaptation. (a,b) Acute thermal response curves for gross photosynthesis and respiration were measured for each isolated autotroph from streams spanning average temperatures from 7 ºC (blue) to 27 ºC (red). Fitted lines are based on the best-fit parameters from non-linear least squares regression using the modified Sharpe-Schoolfield model (see Methods). (c) Metabolic rates normalised to 10 ºC, $b(T_c)$, decrease exponentially with increasing stream temperature for gross photosynthesis (green), net photosynthesis (blue) and respiration (red) (d) Rates of gross photosynthesis at the average stream temperature showed no temperature dependence. Fitted lines and coloured bands in (c) and (d) represent the best fit and the uncertainty of the fixed effects of the best linear mixed effect model.

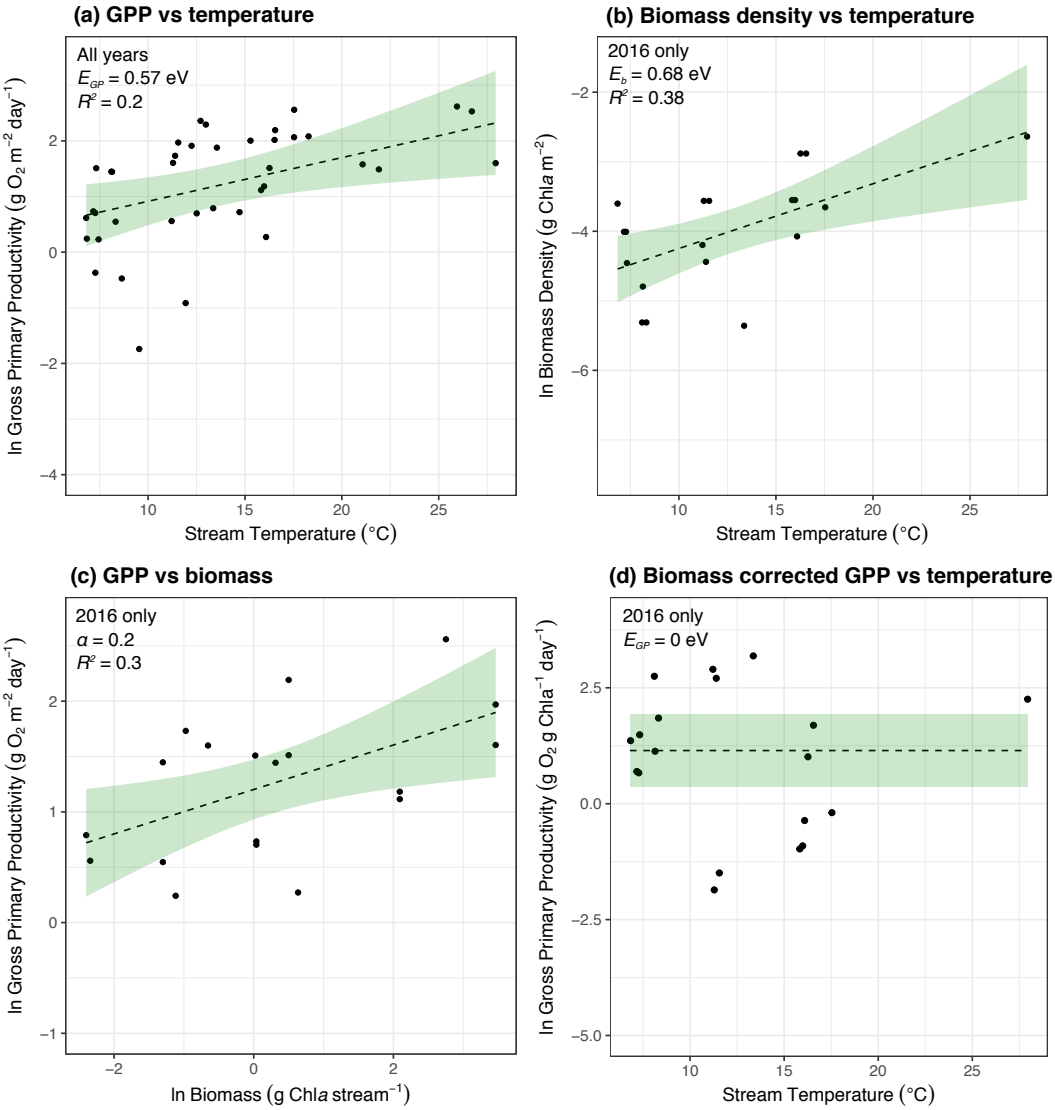

Figure 3 | The effects of temperature and biomass on gross primary productivity. Gross primary productivity (a) and biomass density (b) increase with temperature across the catchment. (c) A multiple regression shows that variation in GPP is driven primarily by changes in biomass. (d) After accounting for biomass, rates of GPP are invariant with respect to temperature across the catchment. Fitted lines in (a, c, d) represent the best fit and the uncertainty of the fixed effects of the best linear mixed effect model (Table 1). In (b) the lines represent the fitted line and associated confidence interval of a linear regression.

751 **Table 1 | Results of the linear mixed effects model analysis for gross primary**
752 **productivity (GPP) for all years and 2016 only.** The results of the model selection
753 procedure on the fixed effect terms are given and the most parsimonious models are
754 highlighted in bold. Analyses reveal that GPP increased significantly with stream
755 temperature. The analyses for 2016 show that the observed temperature response was
756 driven by covariance between biomass and temperature rather than the direct effects
757 of temperature on rates of photosynthesis *per se*.

Model	d.f.	AICc	log Lik	L-ratio	P
All years :					
random effects structure random = 1 | stream/year/day					
fixed effects structure					
1. ln *GPP* ~ 1 + stream temperature	**6**	**82.9**	**-34.0**		
2. ln flux ~ 1	5	85.8	-36.9	5.80	**0.016**
2016 only :					
random effects structure random = 1 | stream/day					
fixed effects structure					
1. ln *GPP* ~ 1 + stream temperature + biomass	6	48.8	-14.9		
2. ln *GPP* ~ 1 + biomass	**5**	**45.3**	**-15.3**	0.87	0.35
3. ln flux ~ 1	4	45.8	-17.4	4.25	**0.04**

758

759

SUPPLEMENTARY INFORMATION

for

Thermal adaptation constrains the temperature dependence of ecosystem metabolism

Daniel Padfield[1], Chris Lowe[1,2*], Angus Buckling[1,2], Richard Ffrench-Constant[2], Simon Jennings[3,4], Felicity Shelley[5], Jón S. Ólafsson[6] & Gabriel Yvon-Durocher[1*]

Author affiliations:

[1] Environment and Sustainability Institute, University of Exeter, Penryn, Cornwall, TR10 9EZ, U.K.

2 Centre for Ecology and Conservation, College of Life and Environmental Sciences, University of Exeter, Penryn, Cornwall, TR10 9FE, U.K.

3 Centre for Environment, Fisheries and Aquaculture Science, Lowestoft, NR33 0HT, U.K.

4 School of Environmental Sciences, Norwich Research Park, University of East Anglia, Norwich, NR4 7TJ, U.K.

5 School of Biological and Chemical Sciences, Queen Mary University of London, London, E1 4NS, U.K.

6. Marine and Freshwater Research Institute, Árleyni 22, 112 Reykjavik, Iceland.

Corresponding authors: Gabriel Yvon-Durocher (g.yvon-durocher@exeter.ac.uk) or Chris Lowe (c.lowe@exeter.ac.uk)

Section 1. Supplementary Tables and Figures

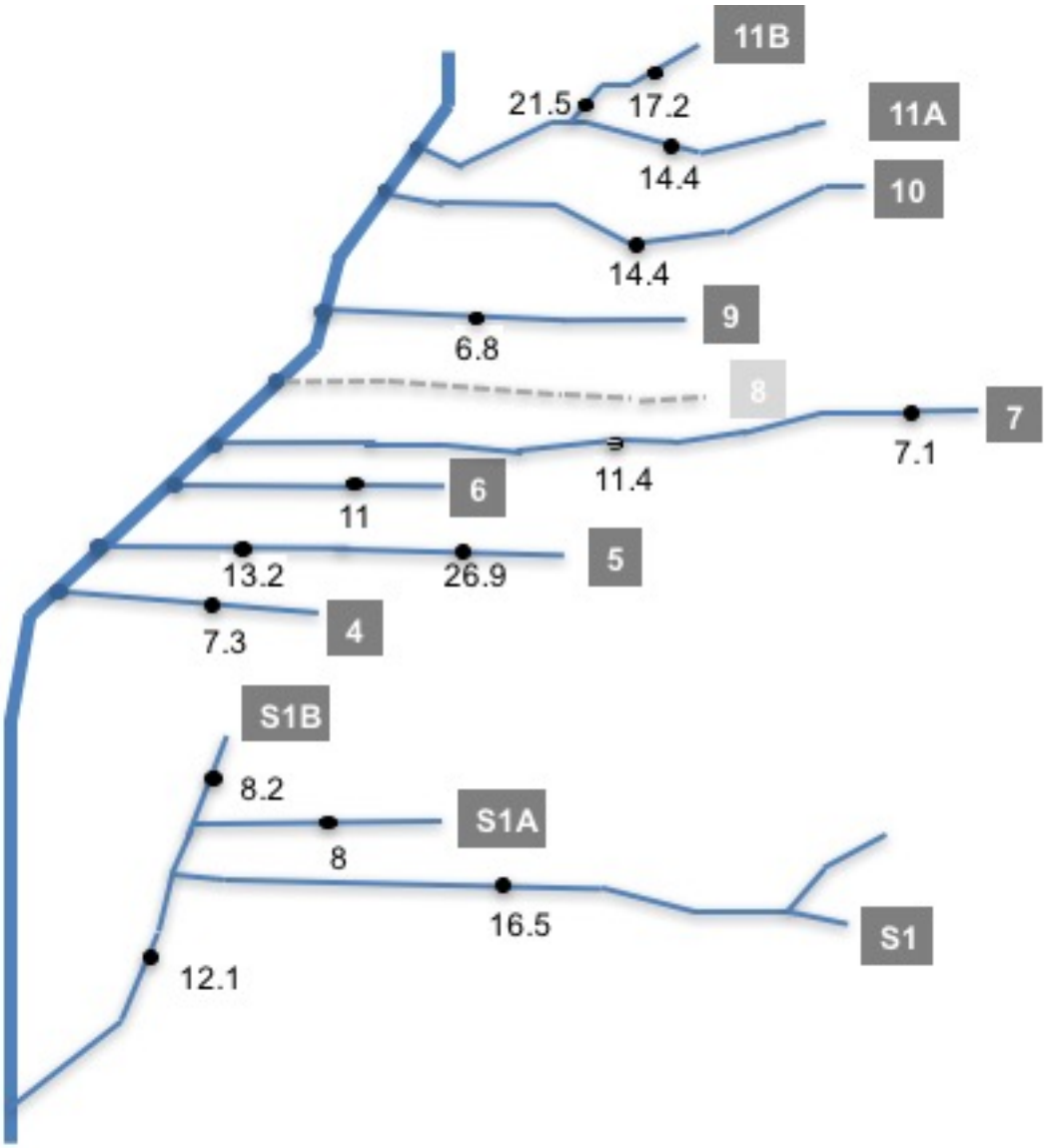

Figure S1. Map of the geothermal stream system in a valley near Hveragerdi, SW Iceland. Temperatures measured a various locations across the catchment are also given.

793 **Table S1.** Mean, minimum and maximum temperature values averaged across days
794 and years (May 2015, May 2016) in the 15 sites. Values are based on a temperature
795 estimates taken at 1 minute intervals. The streams are listed with increasing mean
796 temperature.
797

798

	Temperature (ºC)		
Stream	Mean	Minimum	Maximum
S9	6.8	5.3	7.9
S7 : high	7.1	6.7	7.9
S4	7.3	5.1	8.9
S1A	8	4.5	11.8
S1B	8.2	7.1	9.7
S6	11	7.3	14.1
S7 : low	11.4	10.4	12.1
S1 : low	12.1	9.7	16.3
S5 : low	13.2	12.1	14.8
S10	14.4	10.4	16.9
S11A	14.4	12.4	16.6
S1 : high	16.5	13.3	18.8
S11B : high	17.2	14.7	19.6
S11B : low	21.5	19.8	23.4
S5 : high	26.9	24.8	28.6

Table S2. Key physical and chemical features of the 15 sites investigated

stream	width (m)	depth (m)	velocity (m s^{-1})	pH	conductivity (µS m^{-1})	nutrients (µmol L^{-1})			
						NO_2	NO_3	NH_4	PO_4
S9	0.41	0.027	0.11	7.57	173.3	0.29	0.23	0.27	0.86
S7 : high	0.4	0.053	0.3	7.43	359.1	0.22	0.44	0.28	0.7
S4	0.46	0.06	0.36	7.27	204.6	0.2	0.08	0.22	0.14
S1A	0.59	0.07	0.5	7.40	230.9	0.25	0.4	0.7	0.54
S1B	0.42	0.058	0.14	7.50	462.4	0.28	0.25	0.18	0.17
S6	0.19	0.029	0.12	7.43	289.6	0.22	0.4	0.21	1.02
S7 : low	0.3	0.043	0.4	7.43	304.7	0.22	0.44	0.28	0.7
S1 : low	1.1	0.13	0.81	7.36	305.2	0.26	0.26	0.48	0.35
S5 : low	0.32	0.041	0.09	7.63	273.6	0.22	0.57	0.17	0.14
S10	0.22	0.109	0.24	7.53	167.0	0.35	-	0.24	0.74
S11A	0.71	0.078	0.77	7.17	235.7	0.24	0.29	0.19	0.55
S1 : high	0.74	0.12	0.61	7.20	321.7	0.26	0.26	0.48	0.35
S11B : high	0.31	0.042	0.33	7.33	407.9	0.25	0.25	0.27	1.25
S11B : low	0.4	0.042	0.33	7.33	407.9	0.25	0.25	0.27	1.25
S5 : high	0.17	0.037	0.06	7.63	319.2	0.22	0.57	0.17	0.27

Table S3. Pearson correlation coefficients between temperature and physical and chemical variables

1

Variable	*r*	P value
width	-0.14	0.56
depth	0.07	0.77
velocity	0.04	0.87
pH	-0.03	0.91
conductivity	-0.02	0.92
NO_2	-0.001	0.47
NO_3	0.18	0.47
NH_4	-0.19	0.44
PO_4	0.07	0.77

Table S4. The photosynthetic traits governing the thermal response curves for the dominant biofilms of each stream.

Stream	Year	Taxon	Net photosynthesis					Respiration					Gross photosynthesis				
			ln $np(T_c)$ (µmol O_2 µg Chla^{-1} h^{-1} @ 10ºC)	E_{np} (eV)	E_h (eV)	T_h (ºC)	T_{opt} (ºC)	ln $r(T_c)$ (µmol O_2 µg Chla^{-1} h^{-1} @ 10ºC)	E_r (eV)	E_h (eV)	T_h (ºC)	T_{opt} (ºC)	ln $gp(T_c)$ (µmol O_2 µg Chla^{-1} h^{-1} @ 10ºC)	E_{gp} (eV)	E_h (eV)	T_h (ºC)	T_{opt} (ºC)
S4	2016	Cladophora	3.9	1.03	4.39	30.6	28.48	2.48	1.01	3.78	31.66	29.53	4.2	0.92	9.19	32.49	30.57
S1A	2016	Cladophora	4.74	0.79	2.58	28.33	25.88	3.07	0.64	4.36	37.28	33.97	4.77	0.89	2.71	26.98	24.95
S1A	2016	Nostoc	4.37	0.52	8.77	36.87	34.28	3.14	0.44	4.26	38.83	34.63	4.8	0.47	2.72	35.36	30.71
S4	2015	Cladophora	3.55	0.87	1.78	21.67	21.52	1.71	0.45	17.21	43.78	41.97	3.61	0.53	2.18	30.18	26.1
S7 : high	2016	Cladophora	4.35	0.73	7.04	31.77	29.33	3.85	0.8	2.94	31.06	28.42	4.48	0.93	3.51	28.24	25.99
S7 : high	2016	Nostoc	2.67	0.98	3.57	34.32	32.1	1.27	0.93	1.77	34.12	34.59	3.33	0.62	9.05	38.83	36.43
S7 : high	2015	Feathermoss	1.32	0.77	4.99	34.19	31.44	1.26	0.55	2.13	42.8	38.64	1.99	0.66	8.81	35.6	33.28
S11A	2016	Nostoc	2.67	1.91	5.29	28.47	27.62	1.13	0.71	5.85	45.74	42.79	2.95	1.57	4.37	28.46	27.43
S10	2016	Nostoc	2.68	1.08	9.9	38.53	36.76	-0.66	1.64	3.15	34.74	34.94	3.42	0.85	7.12	38.39	36.06
S1 : high	2016	Nostoc	3.77	1.03	8.87	39.61	37.69	1.33	1.09	3.23	41.01	39.26	4.36	0.85	3.66	37.86	35.15
S11b : high	2015	Feathermoss	1.82	1.12	2.64	24.53	23.64	1.1	0.48	1.64	49.7	45	2.08	1.14	2.5	25.19	24.64
S5 : high	2015	Anabaena	2.58	0.54	5.9	42.5	39.19	0.68	0.66	2.04	39.71	36.65	2.73	0.55	5.69	42.37	39.02
S5 : high	2016	Anabaena	2.66	0.85	4.02	37.4	34.71	0.45	1.58	2.35	29.63	32.12	2.79	0.77	5.63	39.89	37.14

Table S5. Results of a linear effects model analysis for each metabolic trait with fixed effects of stream temperature and metabolic flux (see Methods). Significant models are highlighted in bold.

Metabolic Trait	Effect	d.f.	AIC	Log Lik	L-ratio	P value
$b(T_c)$	~ 1 + stream temperature * metabolic flux	8	96.94	-40.47		
	~ 1 + stream temperature + metabolic flux	6	94.89	-41.43	1.93	0.37
	~ 1 + metabolic flux	5	98.28	-44.14	5.41	**0.02**
E_a	~ 1 + stream temperature * metabolic flux	8	37.03	-10.51		
	~ 1 + stream temperature + metabolic flux	6	36.36	-12.18	3.33	0.189
	~ 1 + stream temperature	4	34.41	-13.21	2.05	0.36
	~ 1	3	32.92	-13.46	0.51	0.48
E_h	~ 1 + stream temperature * metabolic flux	8	72.92	-28.46		
	~ 1 + stream temperature + metabolic flux	6	73.83	-30.91	4.91	0.09
	~ 1 + metabolic flux	5	72.07	-31.04	0.24	0.62
	~ 1	3	71.37	-32.68	3.30	0.19
T_h	~ 1 + stream temperature * metabolic flux	8	-192.08	104.04		
	~ 1 + stream temperature + metabolic flux	6	-192.92	102.46	3.15	0.206
	~ 1 + metabolic flux	5	-190.32	100.16	4.60	**0.032**
T_{opt}	~ 1 + stream temperature * metabolic flux	8	-27.21	21.61		
	~ 1 + stream temperature + metabolic flux	6	-28.72	20.36	2.49	0.29
	~ 1 + metabolic flux	5	-24.54	17.27	6.18	**0.013**
$b(T_s)$	~ 1 + stream temperature * metabolic flux	8	48.64	-16.32		
	~ 1 + stream temperature + metabolic flux	6	44.68	-16.34	0.05	0.98
	~ 1 + metabolic flux	5	42.99	-16.49	0.31	0.58
	~ 1	4	64.21	-29.10	25.22	**<0.0001**

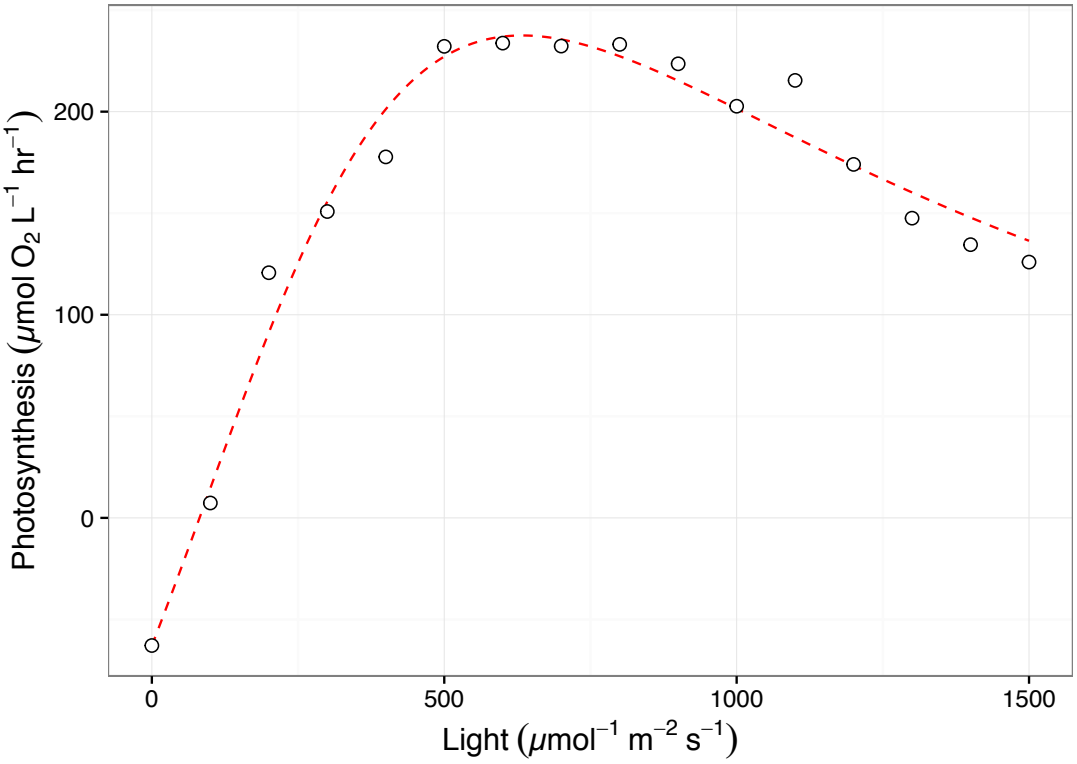

Fig S2. Photosynthesis irradiance curve used to determine optimal light for the acute temperature response of gross photosynthesis. Rates of net photosynthesis were measured at various light intensities at the average stream temperature of each biofilm. Here data are presented for *Nostoc spp.* in stream 7 (high) at 7.1 ºC. Lines represent the best fit to the modified Eiler's model using non-linear least squares regression (See methods).

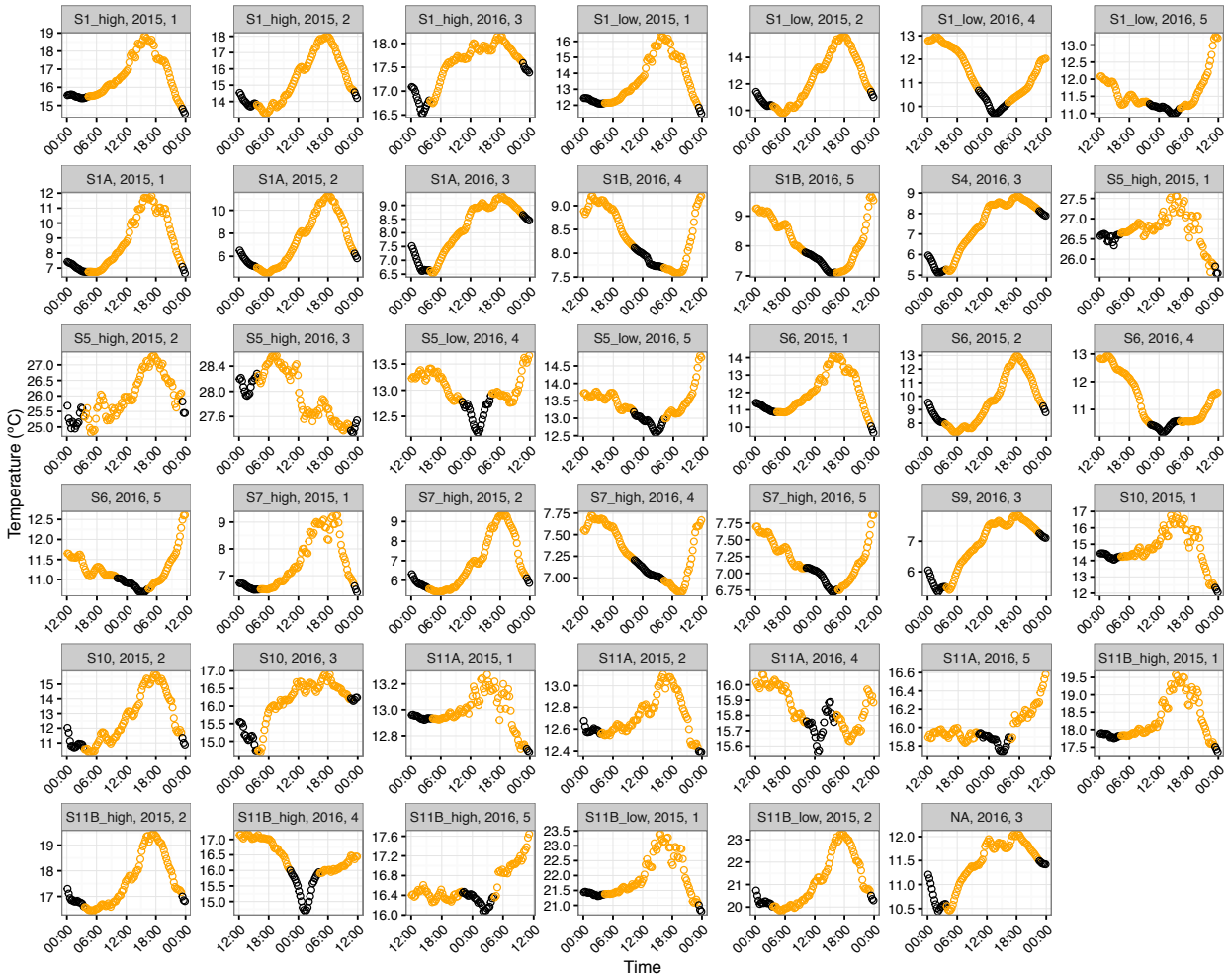

Fig S3. Daily cycles in temperature from each stream across days and years. Each panel is a single day of temperature variation split by each unique stream and across years (2015 or 2016). The data is split into "night" (black points) and "day" (yellow points) by defining night as < 5µmol m^{-2} s^{-1} (see Methods).

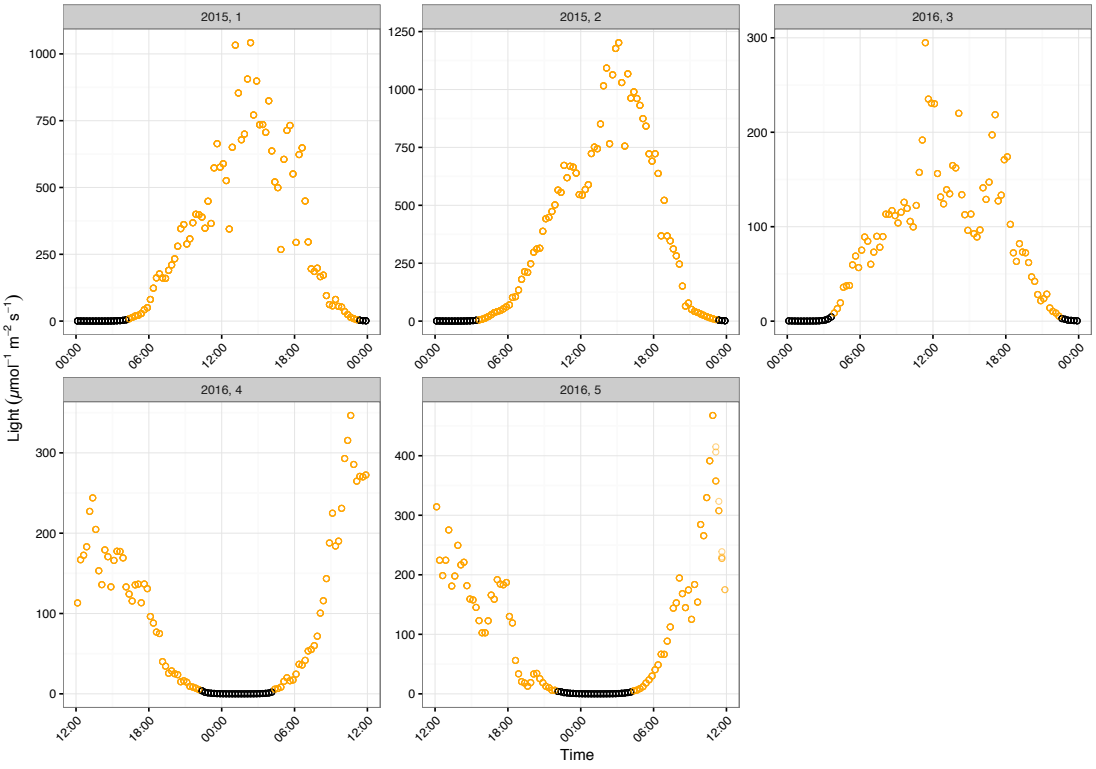

Fig S4. Daily cycles in light from across days and years. Each panel is a single day of light variation split by each unique stream and across years (2015 or 2016). The data is split into "night" (black points) and "day" (yellow points) by defining night as $< 5\mu mol\ m^{-2}\ s^{-1}$ (see Methods).

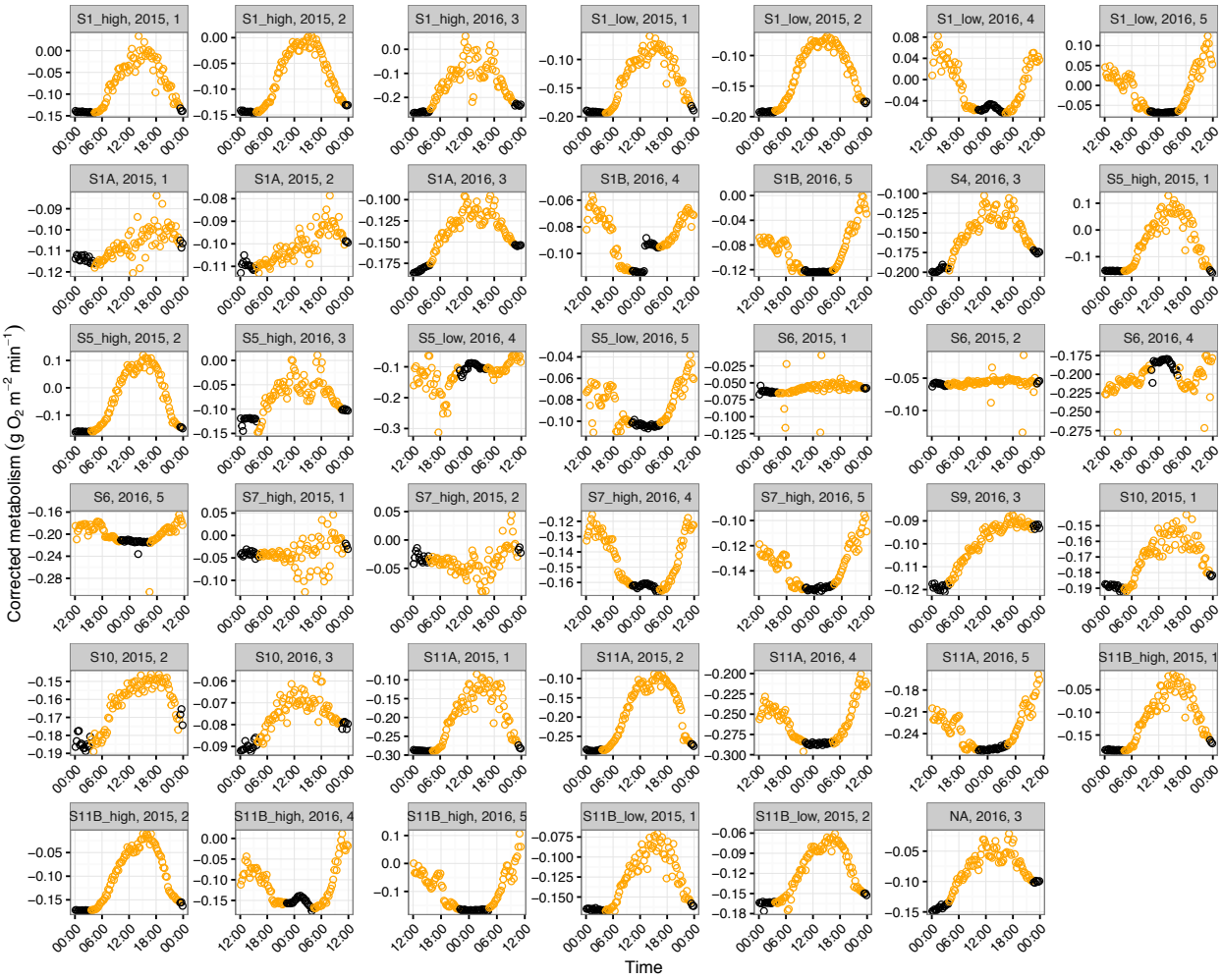

Fig S5. Daily cycles in metabolic flux from each site across days and years. Each panel is a single day of metabolic rate after accounting for reaeration ($\Delta DO - K$; see Methods) split by each unique stream and across years (2015 or 2016). The data is split into "night" (black points) and "day" (yellow points) by defining night as < 5µmol m^{-2} s^{-1} (see Methods).

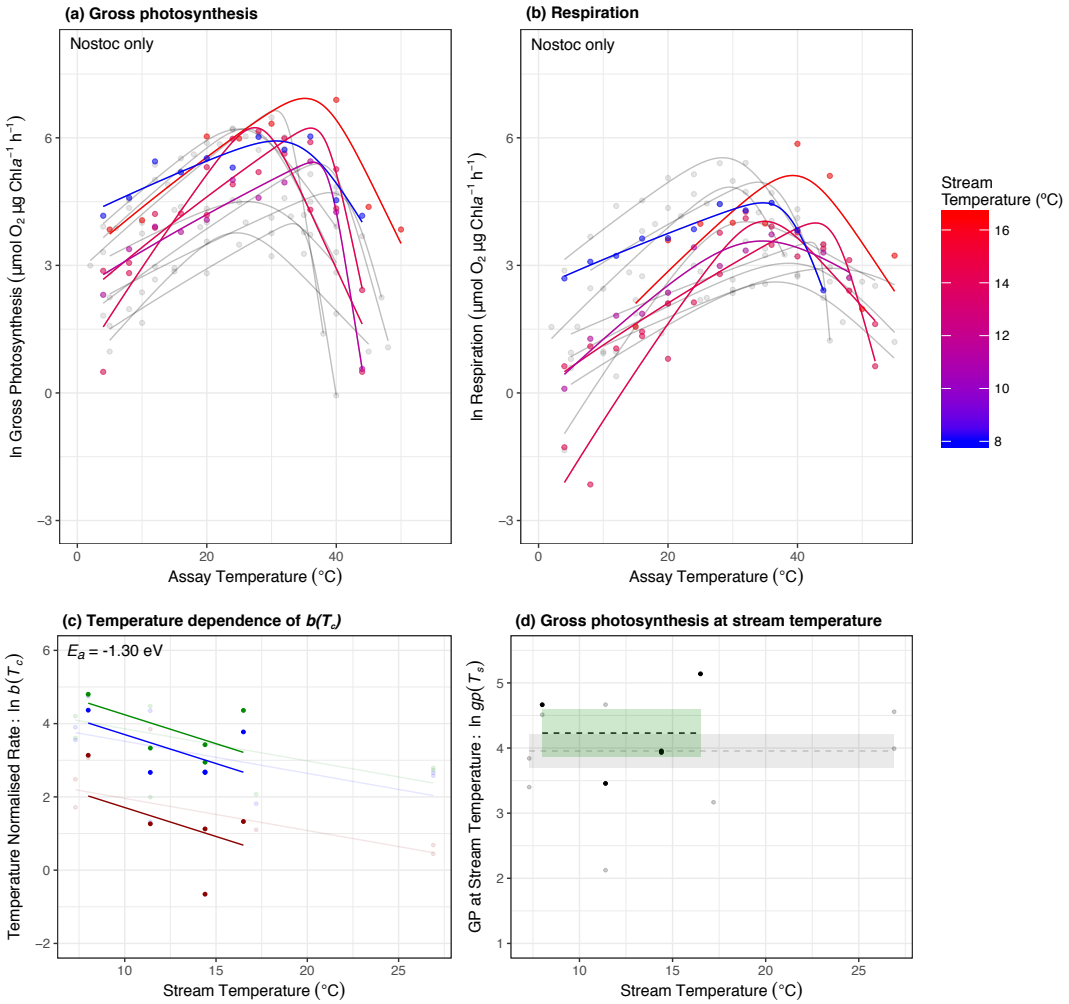

Fig S6. Patterns of thermal adaptation in *Nostoc* spp. only. (a) (a,b) Acute thermal response curves for gross photosynthesis and respiration were measured for each isolated autotroph from streams spanning average temperatures from 7 ºC (blue) to 17 ºC (red) for stream biofilms dominated by *Nostoc* spp. (c) Optimum temperatures were consistently higher than the average stream temperature. (c) Metabolic rates normalised to 10 ºC, $b(T_c)$, decrease exponentially with increasing stream temperature for gross photosynthesis (green), net photosynthesis (blue) and respiration (red). (d) Rates of gross photosynthesis at the average stream temperature showed no temperature dependence. Grey points and lines highlight the other taxa to facilitate direct comparison to the relationship for *Nostoc* spp.

Section 2. Supplementary Methods.

Derivation of the activation energy of net photosynthesis. The rate of net photosynthesis, $np(T)$, at temperature, T, is equal to the difference between the rates of gross photosynthesis, $gp(T)$, and respiration, $r(T)$. Equation 5 (main text) implies that the temperature sensitivity of net photosynthesis will not follow a simple Boltzmann-Arrhenius relationship. Instead, the apparent activation energy of net photosynthesis, E_{np}, can be approximated in the vicinity of T_c as (Yvon-Durocher *et al.* 2014),

$$E_{np} \equiv \frac{dln(np(T))}{d\left(\frac{1}{kT}\right)}_{T=T_c} = \frac{E_{gp}\, gp(T_c) + E_r r(T_c)}{gp(T_c) + r(T_c)} \quad \text{(S1)}$$

which is equal to an average of the activation energies of E_{gp} and E_r, weighted by their respective normalisations, $gp(T_c)$ and $r(T_c)$. Using this approximation, we can then express the temperature dependence of np as

$$np(T) = np(T_c) m^{\alpha} e^{E_{np}\left(\frac{1}{kT_c} - \frac{1}{kT}\right)} \quad \text{(S2)}$$

where $np(T_c) = gp(T_c) - r(T_c)$. We quantified the accuracy of this approximation by comparing E_{np} derived using eq. S1 to the apparent activation energy of net photosynthesis measured by fitting eq. (1) to the net photosynthesis data (see Methods). The derived and measured estimates of E_{np} were positively correlated with a slope that had confidence intervals which overlapped unity (slope = 1.22, 95% CI: 0.78 – 1.65) and R^2 = 0.75 (Fig. S7).

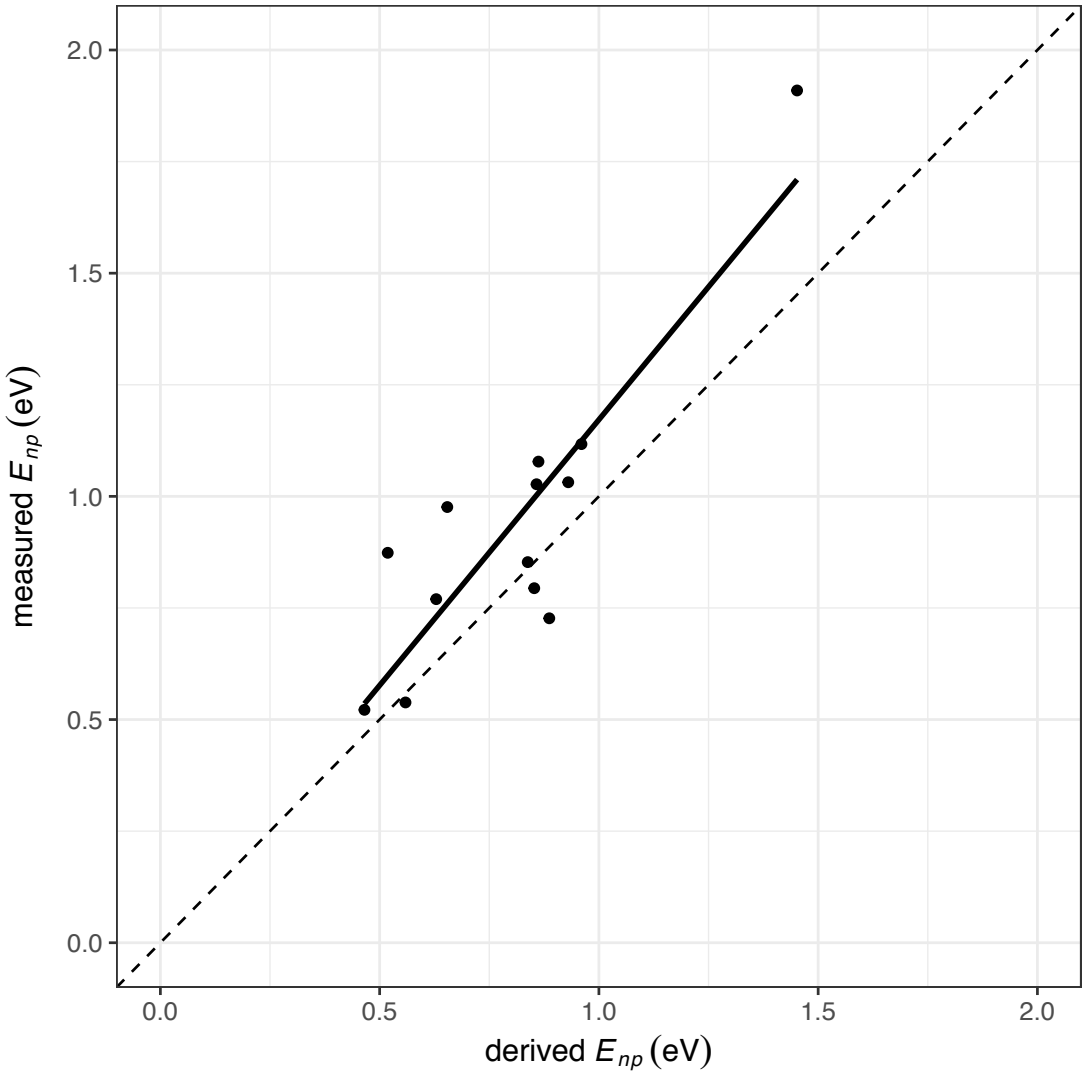

71

72 **Figure S7. Comparison between measured and derived activation energies for**
73 **net photosynthesis.** Activation energies of net photosynthesis measured from fitting
74 the rate data to the modified Sharpe-Schoolfield equation (eq. 1) correlate well with
75 the derived activation energy of net photosynthesis calculated using equation S1. The
76 fitted line is the best fit of a linear model and the 1:1 line is shown for comparison.

77

78

79 **Comparison of measured and modelled reaeration rates.** To assess the robustness
80 of our modelled values of reaeration, we compared measurements of the reaeration
81 rate made in nearby streams in Iceland with comparable physical characteristics using
82 propane additions (from Demars *et al.* 2011), to values estimated using the surface
83 renewal model (eq. 14, main text). In Demars *et al.* (2011), the reaeration rate was
84 measured using a tracer study, where propane was bubbled continuously across the
85 width of the stream at an upstream station. Water samples were taken at a downstream
86 station and analysed by gas chromatography back in the laboratory (see for a more
87 detailed description of the methods). The change in propane concentration the over
88 the reach and the travel time were used to estimate the reaaeration rate, K (min^{-1}).
89 We compared the measured values of reaeration, K (min^{-1}), from Demars *et al.*
90 (2011) to estimated values of K derived Eq. 14 (main text) and measurements of
91 velocity, depth and temperature for those streams. We found a strong correlation
92 between modelled and measured values of K with 95% confidence intervals on the
93 slope that included unity (slope = 1.13, 95% CI: 0.76 – 1.50) and an $R^2 = 0.61$ (Fig.
94 S8). Consequently, we are confident that estimates of reaeration derived from the
95 surface renewal model are robust for the streams included in our survey.
96

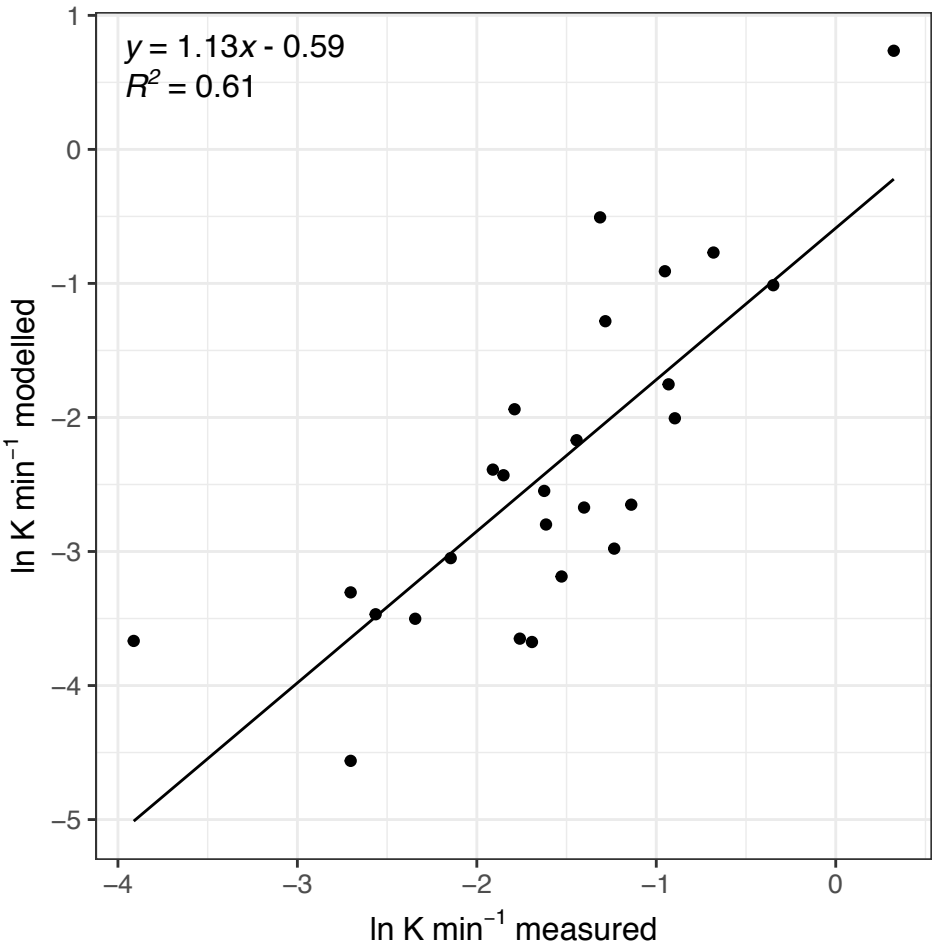

Figure S8. Comparison of modelled and measured rates of reaeration. Rates of measured reaeration using a propane tracer study are positively correlated with those derived using the surface renewal model (eq. 14; main text) with slope that was statistically indistinguishable from unity.